

Two-Photon Macromolecular Probe Based on a Quadrupolar Anthracenyl Scaffold for Sensitive Recognition of Serum Proteins under Simulated Physiological Conditions

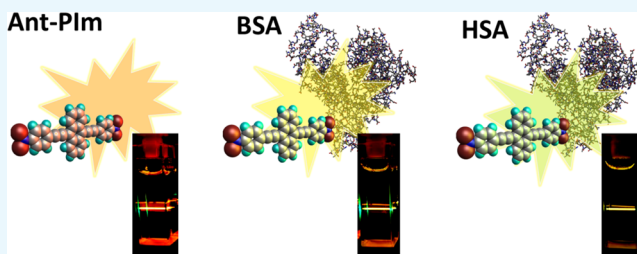
Marco Deiana,[†] Bastien Mettra,[‡] Leszek M. Mazur,[†] Chantal Andraud,[‡] Marek Samoc,[†] Cyrille Monnereau,^{*,‡} and Katarzyna Matczyszyn^{*,†}

[†]Advanced Materials Engineering and Modelling Group, Faculty of Chemistry, Wrocław University of Science and Technology, Wyb. Wyspińskiego 27, 50-370 Wrocław, Poland

[‡]Univ Lyon, Ens de Lyon, CNRS UMR 5182, Université Lyon 1, Laboratoire de Chimie, F69342 Lyon, France

Supporting Information

ABSTRACT: The binding interaction of a biocompatible water-soluble polycationic two-photon fluorophore (**Ant-PIIm**) toward human serum albumin (HSA) was thoroughly investigated under simulated physiological conditions using a combination of steady-state, time-resolved, and two-photon excited fluorescence techniques. The emission properties of both **Ant-PIIm** and the fluorescent amino acid residues in HSA undergo remarkable changes upon complexation allowing the thermodynamic profile associated with **Ant-PIIm**–HSA complexation to be accurately established. The marked increase in **Ant-PIIm** fluorescence intensity and quantum yield in the proteinous environment seems to be the outcome of the attenuation of radiationless decay pathways resulting from motional restriction imposed on the fluorophore. Fluorescence resonance energy transfer and site-marker competitive experiments provide conclusive evidence that the binding of **Ant-PIIm** preferentially occurs within the subdomain IIA. The pronounced hypsochromic effect and increased fluorescence enhancement upon association with HSA, compared to that of bovine serum albumin (BSA) and other biological interferents, makes the polymeric **Ant-PIIm** probe a valuable sensing agent in rather complex biological environments, allowing facile discrimination between the closely related HSA and BSA. Furthermore, the strong two-photon absorption (TPA) with a maximum located at 820 nm along with a TPA cross section $\sigma_2 > 800 \text{ GM}$, and the marked changes in the position and intensity of the band upon complexation definitely make **Ant-PIIm** a promising probe for two-photon excited fluorescence-based discrimination of HSA from BSA.



1. INTRODUCTION

The archetypical human serum albumin (HSA) is the main extracellular protein of the circulatory system.^{1–3} In particular, the ability of HSA to interact with a wide range of endogenous metabolites and exogenous drugs, which may modify their pharmacokinetic and pharmacodynamic properties and influence their distribution and availability toward the biological target, is well known.^{4–6}

X-ray crystallographic analysis of HSA has revealed that this globular protein, a 585 amino acid residue monomer, consists of three homologous α -helical domains (I–III), each of which is subdivided into two subdomains A and B.⁷ Competitive studies and crystal structure analysis enabled the identification of two specific ligand binding sites within the hydrophobic cavities of the protein template named either subdomains IIA and IIIA or Sudlow's site I and II, respectively, in which molecules acting as HSA probes bind to this biomolecule with association constants ranging from 10^3 to 10^6 M^{-1} .^{8–10} It is known that either a low (hypoproteinemia) or high level (microalbuminuria) of HSA in the blood plasma is a characteristic feature of physical health issues such as cirrhosis,

chronic hepatitis, diabetes, and hypertension.^{11,12} In this context, the selectivity of a probe with respect to binding with HSA or other relevant reactive biological interferents (bovine serum albumin (BSA), myoglobin, lysozyme, chymotrypsin, chymotrypsinogen A, L-cysteine, L-glutathione, and L-arginine) is of great interest for laboratory biomedical analyses. In this article, we were particularly interested in controlling the HSA selectivity over BSA. BSA, which demonstrates 70% of the biological functions of HSA, is widely used as a HSA replacement due to its lower cost in many biochemical and pharmacological assays;^{13–16} the ability to discriminate between these two similar proteins is therefore a challenge of great importance. Although several fluorescent probes for serum albumin detection have been reported, most of them have shown poor selectivity for HSA over BSA and their detection limits were found to be above 30 mg/L.^{17–28} Additionally, their excitation and emission wavelengths often lie in the UV or

Received: May 25, 2017

Accepted: June 28, 2017

Published: September 12, 2017

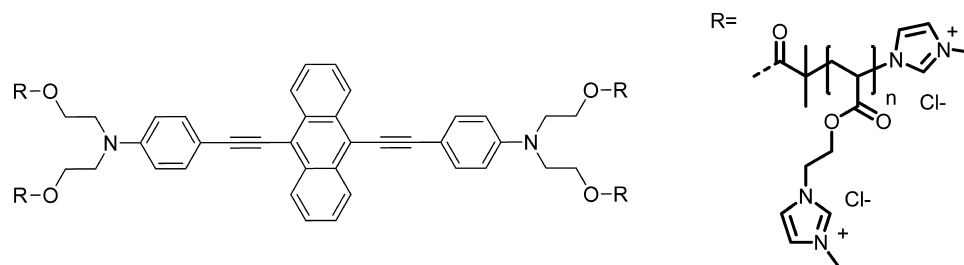


Figure 1. Chemical structure of **Ant-PIm** ($n = 4$ and 5).

visible region of the electromagnetic spectrum, which does not allow easy discrimination from biological autofluorescence. Thus, red emitting probes that can be excited by two-photon absorption (TPA) in the near infrared (NIR) range would constitute a significant improvement over existing systems.

Indeed, the development of new, bright, two-photon fluorescence probes, possessing a relatively high TPA cross section in the NIR region, has received much attention during the last decade due to their promising applications in both laboratory biological imaging and clinical diagnosis.^{29–35} Advantages such as larger penetration depth of the exciting light, low tissue autofluorescence background, reduced photodamage, and photobleaching make two-photon based technologies an advantageous substitute over their one-photon counterparts.^{29–35}

We recently developed a polymer engineering strategy for water-soluble polymer NIR probes with large two-photon excited fluorescence brightness for cellular and intravital two-photon laser scanning microscopy (TPLSM) imaging.^{36–38} From a chemist's point of view, to meet the criteria needed for the development of suitable nonlinear probes useful for in vitro or in vivo cell imaging in tissues, detection of chemical analytes, and monitoring of biological processes with excellent spatial and temporal resolution, requires to address several pivotal points, which were central in our rational molecular engineering approach:^{38–40}

- The molecule should display a large TPA cross section and significant fluorescence quantum yield in the biological transparency window (BTW: 680–1300 nm);
- The molecule should possess good two-photon brightness ($\phi \times \sigma_2$), in the far-red or NIR regions, to be implemented as a microscopic tool in TPLSM procedures;
- The molecule must be water soluble (the majority of nonlinear probes are not soluble in water media due to the extended aromatic surfaces needed to enhance the σ_2 values), biocompatible, and furtive to the immune system to ensure a relatively long residence time within the organism that is compatible with imaging of biological processes;
- The molecule must be nontoxic, affordable at a large scale, and exert good selectivity toward biological targets/compartments.

An overwhelming majority of the aforementioned points were addressed for the neutral macromolecular probes **Ant-PHEA**³⁶ and the quasi-quadrupolar **Ant2-PHEA**,³⁸ which are two of our best-suited reported probes in this regard.

We recently found that **Ant-PHEA** and its analogous cationic (**Ant-PIm**) anthracene polymeric probe, designed using this approach, presented relatively high affinity toward double-stranded DNA, even if the latter seemed to be particularly

sensitive to the surroundings.^{41,42} This overall framework prompted us to investigate the affinity of **Ant-PIm** (Figure 1), whose synthesis has been reported elsewhere,⁴² toward HSA and its selectivity over BSA.

In this contribution, we report the characterization of the HSA–**Ant-PIm** binding mode using a combination of steady-state, time-resolved, and two-photon excited fluorescence techniques. In particular, we provide detailed insights into the affinity constant, binding sites, intermolecular distance, nonlinear optical parameters, and secondary structure changes determining the **Ant-PIm**–HSA association mechanism. Furthermore, the ability of **Ant-PIm** to selectively recognize and discriminate HSA from BSA and common biological interferents is also described, highlighting the outstanding properties of the probe to suitably detect HSA in rather complex biological environments. This is the first report in which a water-soluble nonlinear probe, which can be excited by TPA within the BTW, is used to selectively detect and discriminate serum proteins in rather complex biological environments under simulated physiological conditions.

2. RESULTS AND DISCUSSION

2.1. Effect of Ant-PIm on HSA Fluorescence Spectra.

HSA contains a single tryptophan, Trp-214, and 18 tyrosine (Tyr) residues, which are responsible for its intrinsic fluorescence.⁴³ Trp-214 is located in subdomain IIA within a hydrophobic pocket, whereas the Tyrs are distributed along the whole peptide chain.⁴⁴ Upon excitation at 280 nm, both the tryptophan and Tyr residues are readily excited but most of the fluorescence arises from Trp-214 due to the resonance energy transfer from Tyr to tryptophan.⁴³ However, the excitation wavelength of 293 nm allows only the tryptophan residue to emit fluorescence.⁴³ If **Ant-PIm** interacts with HSA, the fluorescence properties of HSA may be modified depending on the proximity of the ligand to the intrinsic protein fluorophores (Trp and/or Tyr). To determine whether both the tryptophan and Tyr residues are involved in the **Ant-PIm**–HSA association process the protein fluorescence emission spectra were recorded in the absence and in the presence of the anthracenyl derivative using excitation wavelengths of 280 and 293 nm (Figure 2).

Upon addition of increasing concentrations of **Ant-PIm**, a steady decrease in the HSA fluorescence intensity ($\approx 91\%$ at $\lambda_{\text{exc}} = 280$ nm and $\approx 86\%$ at $\lambda_{\text{exc}} = 293$ nm), with a concomitant red shift ($\lambda_{\text{max}}(\lambda_{\text{exc}}=280 \text{ nm}) = 340$ nm and $\lambda_{\text{max}}(\lambda_{\text{exc}}=293 \text{ nm}) = 346$ nm) of the maximum emission wavelength of 8 and 4 nm, respectively, was observed, suggesting that almost quantitative energy transfer from the aa residues to **Ant-PIm** occurs. To provide further insights into the quenching nature of the HSA–**Ant-PIm** complex, the fluorescence data were analyzed using

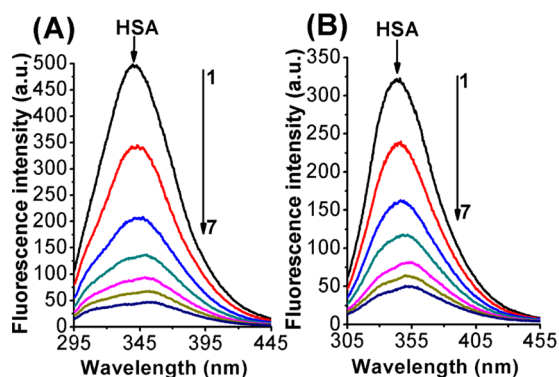


Figure 2. Fluorescence emission spectra of HSA (10.0 μM) treated with: 0.0, 2.5, 5.0, 7.5, 10.0, 12.5, and 15.0 μM (curves 1–7) **Ant-PIm** at 298 K at (A) $\lambda_{\text{exc}} = 280$ nm and (B) $\lambda_{\text{exc}} = 293$ nm.

the Stern–Volmer equation assuming a static binding quenching phenomenon, as discussed in detail further on.^{45,46}

$$\frac{F_0}{F} = 1 + k_q \tau_0 [Q] = 1 + K_S [Q] \quad (1)$$

where F_0 and F denote the steady-state fluorescence intensities in the absence and presence of **Ant-PIm**, respectively. K_S is the Stern–Volmer constant used in the presence of a static quenching mechanism, $[Q]$ is the **Ant-PIm** concentration, k_q is the apparent quenching rate constant of the biomolecules, and τ_0 is the average excited-state lifetime of HSA without a quencher and it is equal to 3.53×10^{-9} s.^{47,48}

Due to **Ant-PIm** absorption at the excitation and emission wavelengths, an inner filter correction was applied before quantitatively analyzing the data using the following equation.⁴⁹

$$F_{\text{corr}} = F_{\text{obs}} \times 10^{(A_{\text{ex}} + A_{\text{em}})/2} \quad (2)$$

where F_{corr} and F_{obs} are the corrected and observed fluorescence, respectively, and A_{ex} and A_{em} are the absorbance values at the excitation and emission wavelengths, respectively.

The plot of F_0/F versus $[\text{Ant-PIm}]$ is shown in Figure 3A.

A significant difference in magnitude of the K_S values ($K_S (\lambda_{\text{exc}}=280\text{nm}) = (6.8 \pm 0.2) \times 10^4 \text{ M}^{-1}$ and $K_S (\lambda_{\text{exc}}=293\text{nm}) = (4.8 \pm 0.3) \times 10^4 \text{ M}^{-1}$) after excitation at these two wavelengths was observed indicating the involvement, to some extent, of the Tyr residues in the molecular interaction between HSA and

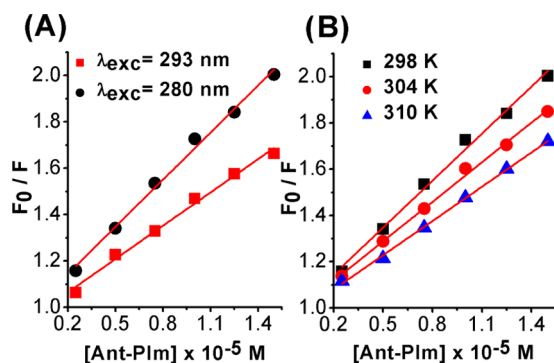


Figure 3. (A) Stern–Volmer plots for the quenching of HSA fluorescence by **Ant-PIm** at 298 K ($\lambda_{\text{exc}} = 280$ nm and 293 K). (B) Stern–Volmer plot for the quenching of HSA fluorescence by **Ant-PIm** at 298, 304, and 310 K ($\lambda_{\text{exc}} = 280$ nm).

Ant-PIm, and this is further confirmed by the Fourier transform infrared (FT-IR) studies discussed further on.

It is known that quenching of the fluorescence intensity can be ascribed to a wide variety of molecular interactions including ground-state complex formation, collisional quenching, excited-state reactions, molecular rearrangement, and energy transfer.⁴⁵ Such different mechanisms are usually collectively considered as either static or dynamic quenching. Static quenching arises from the formation of a ground-state dark complex between the fluorophore (F) and the quencher (Q), whereas dynamic quenching refers to the diffusive encounter between the fluorophore and the quencher during the lifetime of the excited state.

Static and dynamic quenching can be distinguished by their different dependence on temperature.⁴⁵ Higher temperatures lead to faster diffusion and thus larger amounts of collisional quenching, whereas in the case of static quenching, they will typically result in the dissociation of weakly bound complexes. The K_S temperature-dependence analysis (Figure 3B and Table 1) shows that less quenching occurs at higher temperatures strongly pointing toward formation of the **Ant-PIm**–HSA complex through a static mechanism. Further evidence was also provided by analysis of the k_q values, which were found to be much higher than the maximum diffusion collisional quenching rate of various quenchers with biopolymers $\approx 2.0 \times 10^{10} \text{ M}^{-1} \text{ s}^{-1}$, confirming the ground-state complex formation (Table 1).

2.2. Fluorescence Binding Data Analysis. By exploiting the fluorescence titration data and assuming a static quenching event, we evaluated the association constant (K_a) using the modified Stern–Volmer equation⁴⁵

$$\frac{F_0}{\Delta F} = \frac{1}{f_a K_a [Q]} + \frac{1}{f_a} \quad (3)$$

where ΔF is the difference between the total fluorescence in the absence and in the presence of **Ant-PIm** and f_a is the fraction of fluorescence that is accessible to the quencher and is equivalent to the number of binding sites (n).

The plot of $F_0/\Delta F$ versus the inverse of the quencher concentration $[Q]$ is linear, which suggests a single component donor quenching system that would be expected for one major binding mode (Figure 4A). The obtained data listed in Table 1 clearly evidence the accessibility of the fluorophore to the quencher and a moderate binding affinity.

When a guest molecule binds to a set of equivalent sites on a macromolecule, the equilibrium binding constant (K_b) can be further calculated according to the Scatchard equation^{50–52}

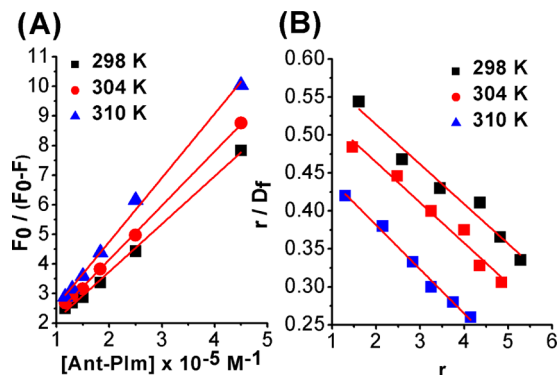
$$\frac{r}{D_f} = nK_b - rK_b \quad (4)$$

where r is the number of ligands attached to a single protein, D_f is the molar concentration of the free ligand, and n refers to the binding site multiplicity per class of binding sites.

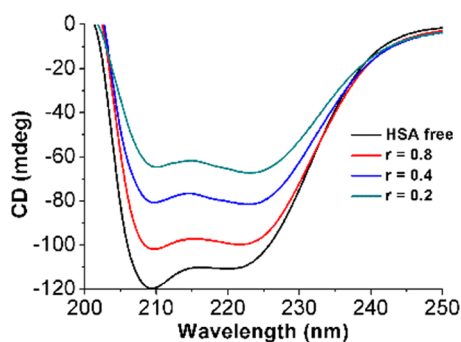
As reported in Table 1, the magnitudes of the binding constants (K_b) are in good agreement with those found using the modified Stern–Volmer plots (K_a) and agree well with literature data on a variety of therapeutic compounds targeting the protein template.^{50,53–55} Furthermore, the linearity of the Scatchard plots (Figure 4B) corroborates well with the aforementioned hypothesis that only one class of binding sites is available to the quencher and it also highlights the noncooperativity of the process.

Table 1. Stern–Volmer (K_S), Quenching Rate Constant (k_q), Association Constants (K_a and K_b), and Number of Binding Sites (n) in the Interaction between Ant-PIm and HSA at Various Temperatures

T (K)	K_S (M^{-1})	k_q ($M^{-1} s^{-1}$)	n	K_a (M^{-1})	K_b (M^{-1})
298	$(6.8 \pm 0.2) \times 10^4$	$(1.9 \pm 0.2) \times 10^{13}$	1.0	$(4.0 \pm 0.3) \times 10^4$	$(5.2 \pm 0.3) \times 10^4$
304	$(5.7 \pm 0.2) \times 10^4$	$(1.6 \pm 0.2) \times 10^{13}$	1.1	$(4.5 \pm 0.2) \times 10^4$	$(5.4 \pm 0.3) \times 10^4$
310	$(4.9 \pm 0.1) \times 10^4$	$(1.4 \pm 0.1) \times 10^{13}$	1.2	$(5.0 \pm 0.2) \times 10^4$	$(5.8 \pm 0.1) \times 10^4$

**Figure 4.** (A) Modified Stern–Volmer plots of the Ant-PIm–HSA association system at 298, 304, and 310 K. (B) Scatchard plots of the Ant-PIm–HSA association system at 298, 304, and 310 K.

2.3. Analysis of Protein Secondary Structure. Changes in the protein secondary structure upon ligand interaction were studied by exploiting the circular dichroism (CD) technique. The HSA CD spectrum consists of one negative dichroic band located in the far UV spectral region, which is characteristic of the α -helical structure of the protein.⁵⁶ Ant-PIm, which is achiral, is thus CD inactive.⁴² Upon addition of Ant-PIm to the HSA solution, a steady decrease in the negative ellipticities at 208 and 222 nm was observed indicating a decrease in the intrinsic HSA α -helix content (Figure 5).

**Figure 5.** CD spectra of HSA (1.0 μ M) treated with: 0.0 (black line), 1.25 (red line), 2.5 (blue line), and 5.0 (green line) μ M Ant-PIm at 298 K.

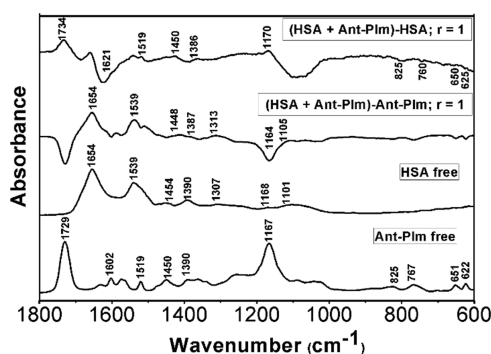
To provide quantitative information on the HSA secondary structure, we calculated the mean residue ellipticity (MRE) value at 208 nm and the α -helix % content using the following equations⁵⁶

$$\text{MRE} = \Theta_{208(\text{mdeg})} / (10 \times n \times l \times C_p) \times 1000 \quad (5)$$

$$\alpha\text{-helix (\%)} = \{(-[\Theta]_{208} - 4000) / (33000 - 4000)\} \times 100 \quad (6)$$

where Θ_{208} is the observed CD value (in millidegrees), C_p is the concentration of the protein, l is the path length of the cuvette, and n is the number of amino acid residues of the protein (585); 4000 is the MRE of the β -sheet and random coil conformation at 208 nm and 33 000 is the MRE of a pure α -helix at 208 nm.

According to the above equations, the percentages of α -helix at different HSA/Ant-PIm molar ratios were calculated. It was found that the HSA α -helix content decreases from 56.8 to 46.2, 33.8, and 24.1% with increasing Ant-PIm concentration ($r = 0.8, 0.4$, and 0.2 , respectively). The CD data categorically established that the presence of the ligand perturbs the protein secondary structure, even if the lack of shift in CD_{max} and the similarity of the intrinsic dichroic protein bands in the absence and in the presence of the ligand suggest that HSA retained its original conformation excluding a denaturation process. To further support our hypothesis, infrared spectroscopic studies were carried out for the free and complexed protein (Figure 6).

**Figure 6.** FT-IR spectra of the free HSA and Ant-PIm and their relative difference FT-IR spectra at a Ant-PIm/HSA molar ratio equal to 1.

As one can easily see, no major spectral shift for the protein amide I band at 1654 cm^{-1} (mainly $\text{C}=\text{O}$ stretch) and amide II band at 1539 cm^{-1} ($\text{N}-\text{H}$ bending coupled with $\text{C}-\text{N}$ stretching mode) could be observed upon ligand interaction. Nevertheless, a decrease in intensity of both the amide bands was detected suggesting a weak overall perturbation of the protein secondary structure due to the reduction in α -helix content, which correlates well with the CD results discussed above.^{55,57–59} It is worth noting that the weak band at 1454 cm^{-1} of the free HSA, assigned to the Tyr side chain vibration, shifted to 1448 cm^{-1} upon ligand addition, which confirms the involvement to some extent of the Tyr residues in the molecular interaction between HSA and Ant-PIm.^{60,61} Further insights into the Ant-PIm–HSA adduct were also provided by analyzing the intrinsic vibrational bands of the anthracenyl derivative. Upon complexation, the bands of the free fluorophore at 1729 and 1167 cm^{-1} (assigned to $\text{C}=\text{O}$ and $\text{C}-\text{O}$ stretching, respectively) shifted to 1734 and 1170 cm^{-1} , respectively, presumably due to the occurrence of external binding interactions, electrostatic in nature, between the

hydrogen bond donor (Tyr 411 and Ser 489) and acceptor sites of the protein and ligand, respectively. Moreover, the free **Ant-PIm** bands at 1602, 1390, and 767 cm^{-1} ascribed to the C–C stretching and C–H bending of the aromatic rings shifted to 1621, 1386, and 760 cm^{-1} , respectively, highlighting the presence of hydrophobic contacts through the anthracenyl polymer aliphatic chain and the surrounding hydrophobic environment in which the tryptophan residue is located, which is in good agreement with the thermodynamic studies reported within the Supporting Information.

2.4. Intermolecular Energy Transfer. The steady-state emission data obtained (vide supra) upon excitation of Trp-214 ($\lambda_{\text{exc}} = 280 \text{ nm}$) suggest the existence of energy transfer from Trp-214 to **Ant-PIm**. Figure 7 shows the overlap between the HSA emission and **Ant-PIm** absorption spectra, respectively.

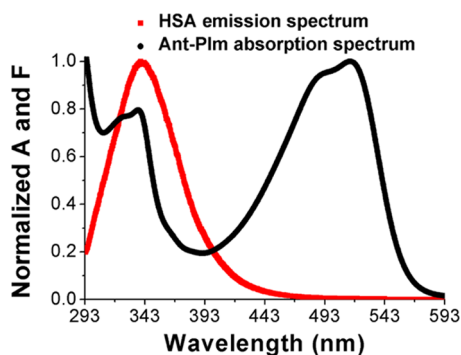


Figure 7. Spectral overlap between the HSA emission and **Ant-PIm** absorption spectra. $[\text{HSA}]/[\text{Ant-PIm}] = 1$.

The Förster equation for nonradiative energy transfer (FRET) can be used to probe the proximity and relative angular orientation between the excited molecule (donor) and its neighbor (acceptor).^{62–64} It is well established that FRET occurs only when all of the following three requirements are fulfilled: (i) the donor (D) is a fluorescence emitter; (ii) the fluorescence emission spectrum of the donor and the absorption spectrum of the acceptor (A) at least partially overlap; and (iii) the distance between D and A is lower than 10 nm.⁴⁰ Under such circumstances, the distance r between HSA (Trp-214) and **Ant-PIm** can be calculated using the following equation⁴⁵

$$E = 1 - \frac{F}{F_0} = \frac{R_0^6}{R_0^6 + r^6} \quad (7)$$

where E and r denote the efficiency of transfer and the average distance between D and A, respectively; R_0 is the critical distance when the energy transfer is 50% and is expressed by the following equation.⁴⁵

$$R_0^6 = 8.79 \times 10^{-25} K^2 n^{-4} \Phi J \quad (8)$$

where K^2 is the orientation factor related to the geometry of the donor and acceptor dipoles in random orientation and its value is equal to 2/3 (which is the approximate case considered here, as we cannot get more precise information); n is the average refractive index of the media; Φ is the fluorescence quantum yield of the donor; and J is the overlap integral between the emission spectrum of the donor and the absorption spectrum of the acceptor and it is defined by the equation given below.⁴⁵

$$J = \frac{\int_0^\infty F_D(\lambda) \varepsilon_A(\lambda) \lambda^4 d\lambda}{\int_0^\infty F_D(\lambda) d\lambda} \quad (9)$$

where $F(\lambda)$ is the corrected fluorescence intensity of the donor in the wavelength range from λ to $\lambda + \Delta\lambda$ and $\varepsilon(\lambda)$ is the extinction coefficient of the acceptor at each λ .

By applying eqs 7–9 and knowing that $n = 1.36$ and $\Phi = 0.118$,^{45,65} we calculated the following parameters: $J = 2.70 \times 10^{-14} \text{ cm}^3 \text{ M}^{-1}$; $E = 0.33$; $R_0 = 2.89 \text{ nm}$; $r = 3.25 \text{ nm}$. As the average distance between donor and acceptor is within the 2–10 nm range and $0.5R_0 < r < 1.5R_0$, these results indicate that the energy transfer from HSA to **Ant-PIm** occurs with high probability and provides further evidence for **Ant-PIm**–HSA complexation through a static quenching mechanism.⁶ The average distance r was found to be in good agreement with those reported for a variety of compounds targeting Sudlow's sites.^{6,50,54,64}

According to the Förster theory, the rate constant of energy transfer (k_{ET}) from Trp-214 to **Ant-PIm** can be estimated by the following equation.⁴⁵

$$k_{\text{ET}} = \tau_{\text{HSA}}^{-1} \times \left(\frac{R_0}{r} \right)^6 \quad (10)$$

where $\tau_{\text{HSA}} = 3.53 \times 10^{-9} \text{ s}$.^{47,48} By implementing the parameters calculated above (eqs 7–9) into the equation, we obtain $k_{\text{ET}} = 1.40 \times 10^8 \text{ s}^{-1}$, which indicates that the energy transfer rate between Trp-214 and **Ant-PIm** is fast enough to compete with the radiative deactivation of the tryptophan residue.^{47,48}

2.5. Effect of HSA on **Ant-PIm** Fluorescence Spectra.

Ant-PIm is a strong luminophore and shows an emission band centered at 570 nm when excited with 516 nm wavelength radiation (Figure 8). Changes in the emission spectra of **Ant-PIm** upon incremental addition of HSA were thus investigated.

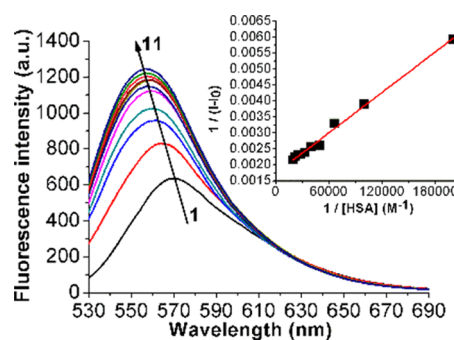


Figure 8. Fluorescence emission spectra of **Ant-PIm** (2.5 μM) at 298 K treated with: 0, 5, 10, 15, 20, 25, 30, 35, 40, 45, and 50 μM (curves 1–11) HSA. Inset: plot of $1/(I - I_0)$ against $1/[\text{HSA}]$ for the **Ant-PIm**–HSA system at 298 K ($\lambda_{\text{exc}} = 516 \text{ nm}$).

Upon incrementally increasing concentrations of HSA, an enhancement in the fluorescence intensity of **Ant-PIm** along with a 14 nm blueshift of the maximum emission wavelength was detected. The enhancement in the fluorescence intensity and change in maximal wavelength can both be ascribed to either (i) the reduction in polarity of the environment around **Ant-PIm** that arises from its interaction with the hydrophobic pocket of the protein or (ii) the accommodation of the **Ant**'s chromophore into the HSA template; this may simultaneously impose a specific conformation on its long conjugated carbon

skeleton, causing modification in the ground and excited-state geometries of the chromophore, and reducing the freedom of rotation of the fluorophore, which in turn, limits the possibility of vibrational deactivation pathways.

To provide quantitative information on the strength of the HSA–**Ant-PIm** interaction, the modified Benesi–Hildebrand equation was used⁶⁶

$$\frac{1}{(I - I_0)} = \frac{1}{(I_\infty - I_0)K_f[\text{HSA}]} + \frac{1}{(I_\infty - I_0)} \quad (11)$$

where I_0 and I are the emission intensities of **Ant-PIm** in the absence and presence of the protein, respectively, and I_∞ is the fluorescence intensity at saturated interaction, which is reached when the excess of added protein in the medium is so large that **Ant-PIm** is exclusively present in its bound form. The plot of $1/(I - I_0)$ versus $1/C_{\text{HSA}}$ is linear over the whole concentration range studied and the binding constant (K_f) can be calculated from the ratio of the intercept and the slope (inset Figure 8) providing a value equal to $(8.5 \pm 0.1) \times 10^4 \text{ M}^{-1}$, which confirms a relatively high binding affinity.

Moreover, by exploiting the linear dependence of the **Ant-PIm** emission changes as a function of HSA concentration, we determined a limit of detection (LOD) ($=3\sigma/\text{slope}$) $= 7.5 \times 10^{-3} \text{ mg/mL}$, which makes **Ant-PIm** an ideal probe to estimate HSA in normal and albuminuria urine samples.²⁶

2.6. Time-Resolved Fluorescence Decay Measurements. To elucidate the origin of the **Ant-PIm** fluorescence enhancement in complex with HSA, the changes in the fluorescence decay functions upon binding to the protein were determined, and are shown in Figure 9.

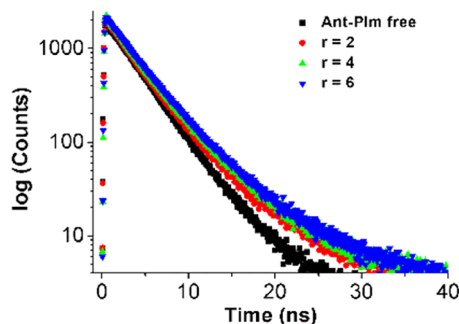


Figure 9. Representative time-resolved fluorescence decay profiles ($\lambda_{\text{exc}} = 515 \text{ nm}$) of **Ant-PIm** at different HSA/**Ant-PIm** molar ratios. $[\text{Ant-PIm}] = 2.5 \mu\text{M}$.

The free **Ant-PIm** was found to exhibit a mono-exponential decay pattern that comprised a slow component of 3.27 ns. However, as reported in Table 2, the time-resolved fluorescence decay of **Ant-PIm** bound to HSA could be satisfactorily described by a bi-exponential pattern with two distinct lifetimes.

Table 2. Time-Resolved Fluorescence Decay Parameters, Fluorescence Quantum Yield, and Kinetic Parameters of Ant-PIm with Increasing Concentrations of HSA

[HSA] (μM)	α_1 (%)	α_2 (%)	τ_1 (ns)	τ_2 (ns)	$\langle\tau\rangle$ (ns)	Φ_f	k_r ($\times 10^7 \text{ s}^{-1}$)	k_{nr} ($\times 10^7 \text{ s}^{-1}$)
0	100		3.27		3.27	0.3	9.17	21.41
5	38	62	2.19	4.16	3.68			
10	40	60	2.31	4.41	3.86			
15	48	52	2.70	4.77	4.06	0.53	13.05	11.58

Upon addition of HSA, the component τ_1 , which corresponds to the free **Ant-PIm** molecule, shows a sudden decrease in magnitude followed by the simultaneous appearance of a new component τ_2 , which provides the largest contribution. The direct outcome of the binding phenomenon between the **Ant**'s chromophore and the protein template can be confirmed by the progressive increase in the average lifetime (τ) with increasing protein concentration.

A more quantitative data analysis was undertaken to demarcate the contribution of the radiative (k_r) and non-radiative (k_{nr}) decay constants of **Ant-PIm** in an aqueous buffer solution and protein environment according to the following equations⁴⁵

$$k_r = \frac{\Phi_f}{\langle\tau\rangle} \quad (12)$$

$$k_r + k_{nr} = \langle\tau\rangle^{-1} \quad (13)$$

where Φ_f denotes the fluorescence quantum yield of **Ant-PIm**. On the basis of the calculated results shown in Table 2, we infer that the longest chromophore lifetime is the direct outcome of the attenuation of the radiationless pathway via the motional restriction imposed on the **Ant-PIm** moiety.

2.7. Unraveling the Selective Ant-PIm Binding to Biological Targets. These results prompted us to investigate whether the revealed emission enhancement upon HSA interaction could be taken advantage of in the conception of a biocompatible fluorescent probe that is able to discriminate HSA from BSA. As shown in Figure 10, an enhancement in

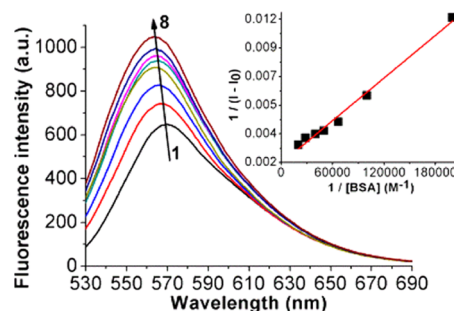


Figure 10. Fluorescence emission spectra of **Ant-PIm** ($2.5 \mu\text{M}$) at 298 K treated with: 0, 5, 10, 15, 20, 25, 35, and $50 \mu\text{M}$ (curves 1–8) of BSA. Inset: plot of $1/(I - I_0)$ against $1/[\text{BSA}]$ for the **Ant-PIm**–BSA system at 298 K.

intrinsic **Ant-PIm** fluorescence intensity with a concomitant 4 nm blueshift of λ_{max} was observed upon BSA addition. Consequently, the reduced hyperchromic and hypsochromic effect observed for the **Ant-PIm**–BSA complex ($K_f^{\text{Ant-PIm-BSA}} = (3.0 \pm 0.3) \times 10^4 \text{ M}^{-1}$) as compared to that of the **Ant-PIm**–HSA adduct allows easy discrimination of HSA from BSA,

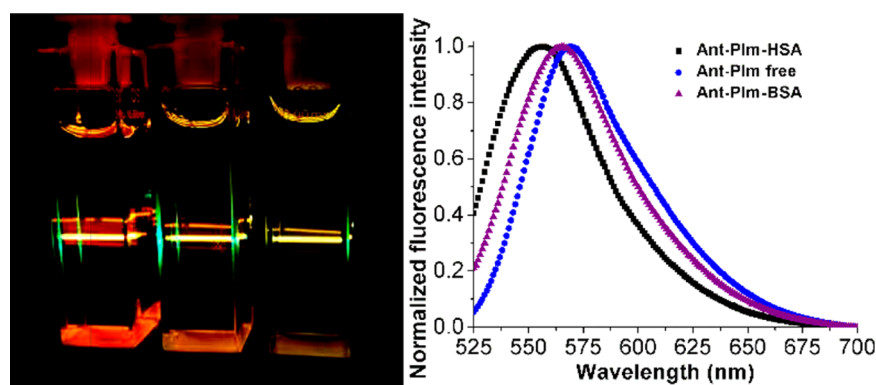


Figure 11. (Left panel) Sensitive discrimination of HSA from BSA by **Ant-PIm** after a 515 nm irradiation. From left to right: free **Ant-PIm** (orangish), **Ant-PIm**–BSA (goldish), and **Ant-PIm**–HSA (yellow-greenish). [**Ant-PIm**] = 2.5 μ M and [BSA] = [HSA] = 15 μ M. (Right panel) Normalized fluorescence intensity responses of **Ant-PIm** in the absence and presence of serum proteins.

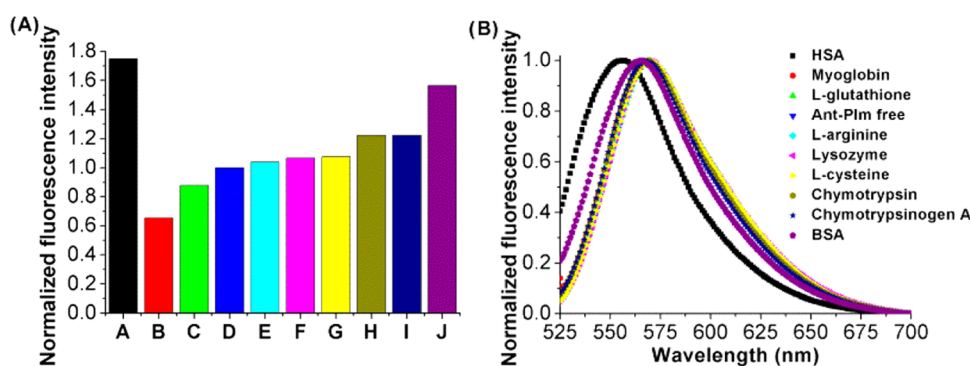


Figure 12. (Left panel A) (A) HSA; (B) Myoglobin; (C) L-glutathione; (D) free **Ant-PIm**; (E) L-arginine; (F) lysozyme; (G) L-cysteine; (H) chymotrypsin; (I) chymotrypsinogen A; (J) BSA. [**Ant-PIm**] = 2.5 μ M and [biological interferents] = 15 μ M. (Right panel B) Normalized fluorescence intensity responses of **Ant-PIm** (2.5 μ M) to HSA, BSA, and other biological interferents (15 μ M).

either by the monitoring of their emission spectra or by naked-eye detection, as shown in Figure 11.

Further insights were also provided by testing the **Ant-PIm**-sensing response toward common biological interferents by fluorescence spectroscopy experiments. As shown in Figure 12, no, or very weak, changes to λ_{max} occurred in the intrinsic **Ant-PIm** emission upon binding to common biomolecules, which highlights the probe's excellent ability to suitably detect HSA in rather complex biological environments.

2.8. Two-Photon Fluorescence Response of the Free Ant-PIm and Ant-PIm–Protein Systems. Recent developments in TPA applications have focused on identifying extrinsic biological targeting agents that are easily excitable by a short pulse light source because they can avoid conventional one-photon drawbacks such as shallow penetration depth, a relatively high autofluorescence background from other naturally occurring emissive compounds, and the tissue photodamage inherent to conventional UV–visible (UV–vis) sources.^{29–35} Consequently, NIR TPA excitable probes, with a high TPA cross section (σ_2), are a much sought-after class of dyes for biomedical imaging, analysis, and diagnosis.^{29–35}

As shown in Figure 13 (top left panel), a relatively high TPA is observed in the spectral region between 780 and 860 nm with the maximum located at 820 nm for both the free and complexed **Ant-PIm**. It is worth noting that the cross section values vary significantly between the unbound ($\sigma_{2\text{Ant-PIm}} = 813$ GM at 820 nm) and bound dye ($\sigma_{2\text{Ant-PIm-HSA}} = 469$ GM and $\sigma_{2\text{Ant-PIm-BSA}} = 443$ GM at 820 nm); therefore, the lack of a common scaling factor for the free and bound **Ant-PIm**

molecule states makes the straightforward comparison of σ_2 values very difficult, as the environmental conditions in which the fluorophore is placed can dramatically modify the transition dipole moment of the dye, affecting the two-photon cross section magnitude. However, if we compare the **Ant-PIm** performance in terms of molecular brightness ($\sigma_2 \times \Phi_f$), we find two similar values for the free fluorophore ($\sigma_{2(\text{Ant-PIm})} \times \Phi_{f(\text{Ant-PIm})} = 244$ GM at 820 nm) and its HSA-bound state ($\sigma_{2(\text{Ant-PIm-HSA})} \times \Phi_{f(\text{Ant-PIm-HSA})} = 248$ GM at 820 nm) (Figure 13 top right panel). These overall findings definitively make the anthracenyl derivative a promising sensing probe for serum protein detection. This was illustrated by irradiating the same cuvettes, as shown in Figure 11, with a Ti:Sapphire laser working at 820 nm: a detectable two-photon excited fluorescence was observed for all three mixtures, underlining even further the potential of **Ant-PIm** for use as a selective probe for the discrimination of HSA versus BSA even in complicated, auto-fluorescent biological mixtures (Figure 13 bottom central panel).

3. CONCLUSIONS

In summary, the HSA-binding properties of a water-soluble fluorophore have been comprehensively investigated under simulated physiological conditions. Steady-state fluorescence data, obtained as a function of temperature, confirmed that hydrophobic forces regulate the **Ant-PIm**–HSA complex formation. Displacement and energy transfer studies provide clear evidence for the binding of **Ant-PIm** in the protein subdomain IIA. CD and FT-IR structural analysis showed a

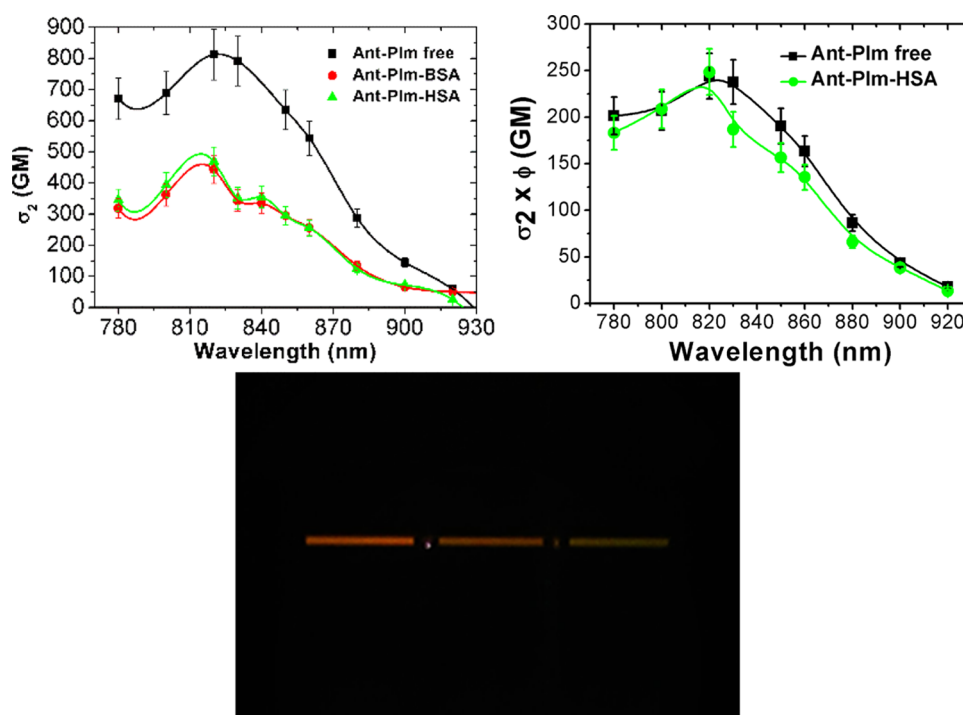


Figure 13. (Top left panel) TPA cross section of **Ant-PIIm** in the absence (black curve) and in the presence of HSA (green curve) and BSA (red curve). [**Ant-PIIm**] = 2.5 μ M and [HSA] = [BSA] = 15 μ M. (Top right panel) Molecular brightness ($\sigma_2 \times \phi_f$) plot of **Ant-PIIm** in the absence (black curve) and presence of HSA (green curve). [**Ant-PIIm**] = 2.5 μ M and [HSA] = 15 μ M. (Bottom central panel) Sensitive discrimination of HSA from BSA by **Ant-PIIm** after a 820 nm irradiation. From left to right: free **Ant-PIIm** (orangish), **Ant-PIIm**–BSA (goldish), and **Ant-PIIm**–HSA (yellow-greenish). [**Ant-PIIm**] = 2.5 μ M and [BSA] = [HSA] = 15 μ M.

decrease in the protein α -helix content upon ligand complexation even if no, or weak, overall changes in the HSA secondary structure were observed. Enhancement of the intrinsic **Ant-PIIm** fluorescence intensity and changes in the fluorophore's lifetime may be considered to be the direct outcome of the attenuation of the radiationless pathway via the motional restriction imposed on the **Ant**'s moiety from the protein template. The different **Ant-PIIm** emission response to HSA and BSA categorically established the excellent selectivity of the probe to suitably target the two similar proteins even in rather complex biosystems, as proven by the lack of response toward common biological interferents. Moreover, the high TPA cross section ($\sigma_2 > 800$ GM) maximum located at 820 nm makes the anthracenyl derivative a promising probe for serum protein discrimination. This is the first report in which a water-soluble two-photon fluorophore has been used for selective albumin detection at physiological pH. We speculate that future works in this area will open up new avenues to develop smart multi-photon anthracenyl-based sensors, which have the potential to emerge as specific bio-markers for diagnostic applications.

4. MATERIALS AND METHODS

4.1. Synthesis of Ant-PIIm. The synthetic route and the physical properties of the anthracenyl derivative **Ant-PIIm** are reported in our previous papers.⁴²

4.2. Reagents. All chemicals used throughout the experiments were purchased from commercial suppliers and used without further purification. HSA and BSA, purchased from Sigma-Aldrich, were diluted in Milli-Q water to a final concentration of 0.2 mM. Stock solutions of Myoglobin, L-glutathione, L-arginine, lysozyme, L-cysteine, chymotrypsin, and chymotrypsinogen A were prepared by dissolving the samples

in Milli-Q water until the desired concentration was reached. Sodium cacodylate trihydrate (0.05 M), supplied by Sigma-Aldrich, was used to control the pH of the solutions (pH 7.2).

4.3. Apparatus and Methods. Absorption spectra were recorded on a PerkinElmer Lambda 20 UV–vis spectrometer. Emission spectra were obtained with a Hitachi F-4500 spectrofluorometer equipped with a xenon lamp. Fluorescence lifetimes were determined with an Edinburgh Instruments FLS 980 spectrophotometer via time-correlated single-photon counting (TCSPC), with excitation from a 516 nm picosecond laser diode. Two-photon excited fluorescence (TPEF) was achieved with a coherent chameleon laser that delivered a train of ≈ 100 fs pulses with 80 MHz repetition rate. The TPEF spectra were recorded by an Ocean Optics 2000 fiber spectrometer. CD experiments were conducted on a Jasco J-815 spectropolarimeter (Jasco Inc). The infrared spectra were collected on a diamond crystal surface under vacuum (<1 hPa) using a Bruker Vertex70v FT-IR spectrometer. Quartz cells with a 1 cm path length were used throughout the measurements.

Titration experiments were recorded keeping the final volume of each solution constant to reduce dilution issues and thus achieve better reproducibility of the recorded data.

4.4. Steady-State Fluorescent Measurements. Fluorescence quenching studies were recorded at different temperatures (298, 304, and 310 K) keeping the HSA concentration constant (10 μ M; $\lambda_{\text{exc}} = 280$ nm or $\lambda_{\text{exc}} = 293$ nm) and varying that of the anthracenyl derivative **Ant-PIIm** until saturation was achieved.

The intrinsic **Ant-PIIm** emission response toward biomolecules was observed at a fixed **Ant-PIIm** concentration (2.5 μ M; $\lambda_{\text{exc}} = 516$ nm) and varying that of the biological targets.

The resulting changes in the emission profiles were used to calculate the biophysical and thermodynamic parameters as well as the strength of binding.

Moreover, the linear dependence of the fluorescence emission of **Ant-PIIm** in the presence of increasing concentrations of HSA allowed the LOD to be estimated, which was defined as: $\text{LOD} = 3\sigma/k$, where σ is the standard deviation of the blank measurement and k is the slope of the linear plot obtained by casting the changes in the fluorescence intensity of the **Ant-PIIm**–HSA complex as a function of HSA concentration.^{26,67,68}

4.5. Fluorescent Displacement Assay. Site-marker competition experiments were performed using the well known serum protein binders Ibuprofen and Warfarin purchased from Sigma-Aldrich. An equimolar concentration of both drugs and HSA was mixed and the relative product was scanned in the wavelength range 285–500 nm ($\lambda_{\text{exc}} = 280$). The resulting signal was normalized to 100% of the emission profile. Subsequently, various concentrations of **Ant-PIIm** were added to the mixture and the fluorescence was measured after an incubation time of 10 min. The addition of **Ant-PIIm** was continued until the fluorescence signal reached saturation. The study, which allowed us to conclude that **Ant-PIIm** could efficiently replace both binders, is included as [Supplementary Material](#).

4.6. Time-Resolved Fluorescence. Fluorescence decay traces of both the free **Ant-PIIm** and its bound state were recorded via TCSPC. The fluorescence was collected at a 90° geometry after passing through a polarizer set at the magic angle. Calculations of **Ant-PIIm** excited-state lifetimes (τ_i) and the corresponding amplitude (A_i) were made using OriginPro 8 software. The amplitude-weighted fluorescence lifetime was calculated using the following formula

$$\langle \tau \rangle = \sum_{i=1}^n A_i \times \tau_i \quad (14)$$

where n denotes the number of decay components in the total function.

4.7. TPEF. TPEF measurements were performed at HSA or BSA/**Ant-PIIm** molar ratios $r = 0$ and 6 using fluorescein as the reference. The relative concentration was adjusted so that the linear absorbance at $2h\nu$ was kept below 0.1 over the whole wavelength range studied (780–920 nm).

The TPA cross section was determined according to the following equation

$$\sigma_2 = \frac{F n_r c_r \phi_r}{F_{\text{ref}} c \phi} \sigma_{2r} \quad (15)$$

where σ_2 is the TPA cross section, c and n are the concentration and refractive index, respectively, and F is the integrated area obtained from the TPEF spectrum. The subscript r refers to the reference solution.

4.8. CD Spectroscopy. CD spectra were recorded as an average of five scans within the wavelength range 200–500 nm. The **Ant-PIIm**/HSA molar ratios were varied from 0 to 5 and the buffer contribution subtracted from each recorded spectrum. Quantitative analysis of the protein secondary structure was performed according to previous reports.⁶⁹

4.9. FT-IR Spectroscopic Measurements. IR measurements were carried out at a fixed HSA/**Ant-PIIm** ratio ($r = 1$) and the relative signal of either the free HSA or **Ant-PIIm** was

subtracted from the HSA–**Ant-PIIm** complex spectrum to achieve only the contribution of the interaction.

■ ASSOCIATED CONTENT

§ Supporting Information

The Supporting Information is available free of charge on the ACS Publications website at DOI: [10.1021/acsomega.7b00665](https://doi.org/10.1021/acsomega.7b00665).

Equilibrium fraction, thermodynamic analysis, and site-marker competitive experiments ([PDF](#))

■ AUTHOR INFORMATION

Corresponding Authors

*E-mail: cyrille.monnereau@ens-lyon.fr (C.M.).

*E-mail: katarzyna.maczyszyn@pwr.edu.pl (K.M.).

ORCID

Marek Samoc: 0000-0002-5404-2455

Cyrille Monnereau: 0000-0002-8928-2416

Katarzyna Matczyszyn: 0000-0001-8578-8340

Author Contributions

The manuscript was written through contributions of all authors. All authors have given approval to the final version of the manuscript.

Notes

The authors declare no competing financial interest.

■ ACKNOWLEDGMENTS

The financial support from the Foundation for Polish Science (FNP) Mistrz grant, NCN OPUS project DEC-2013/09/B/ST5/03417, and a statutory activity subsidy from the Polish Ministry of Science and Higher Education for the Faculty of Chemistry of WUT are acknowledged. The Leading National Research Centre (KNOW), Wrocław Centre of Biotechnology programme, provided funding for open access of the paper.

■ REFERENCES

- (1) Kumar, C. V.; Buranaprapuk, A. Site-Specific Photocleavage of Proteins. *Angew. Chem., Int. Ed.* **1997**, *36*, 2085–2087.
- (2) Peters, T., Jr. Serum Albumin. *Adv. Protein Chem.* **1985**, *37*, 161–245.
- (3) Carter, D. C.; Ho, J. X. Structure of Serum Albumin. *Adv. Protein Chem.* **1994**, *45*, 153–203.
- (4) Lázaro, E.; Lowe, P. J.; Briand, X.; Faller, B. New Approach to Measure Protein Binding Based on a Parallel Artificial Membrane Assay and Human Serum Albumin. *J. Med. Chem.* **2008**, *51*, 2009–2017.
- (5) Nicoletti, F. P.; Howes, B. D.; Fittipaldi, M.; Fanali, G.; Fasano, M.; Ascenzi, P.; Smulevich, G. Ibuprofen Induces an Allosteric Conformational Transition in the Heme Complex of Human Serum Albumin with Significant Effects on Heme Ligation. *J. Am. Chem. Soc.* **2008**, *130*, 11677–11688.
- (6) Abou-Zied, O. K.; Al-Shihi, O. I. K. Characterization of Subdomain IIA Binding Site of Human Serum Albumin in Its Native, Unfolded, and Refolded States Using Small Molecular Probes. *J. Am. Chem. Soc.* **2008**, *130*, 10793–10801.
- (7) He, X. M.; Carter, D. C. Atomic Structure and Chemistry of Human Serum Albumin. *Nature* **1992**, *358*, 209–215.
- (8) Sudlow, G.; Birkett, D. J.; Wade, D. N. The Characterization of Two Specific Drug Binding Sites on Human Serum Albumin. *Mol. Pharmacol.* **1975**, *11*, 824–832.
- (9) Sudlow, G.; Birkett, D. J.; Wade, D. N. Further Characterization of Specific Drug Binding Sites on Human Serum Albumin. *Mol. Pharmacol.* **1976**, *12*, 1052–1061.
- (10) Zsila, F.; Bikadi, Z.; Malik, D.; Hari, P.; Pechan, I.; Berces, A.; Hazai, E. Evaluation of Drug-Human Serum Albumin Binding

Interactions with Support Vector Machine Aided Online Automated Docking. *Bioinformatics* **2011**, *27*, 1806–1813.

(11) Hoogenberg, K.; Sluiter, W. J.; Dullart, R. P. F. Effect of Growth Hormone and Insulin-like Growth Factor I on Urinary Albumin Excretion: Studies in Acromegaly and Growth Hormone Deficiency. *Acta Endocrinol.* **1993**, *129*, 151–157.

(12) Murch, S. H.; Winyard, P. J. D.; Koletzko, S.; Wehner, B.; Cheema, H. A.; Risdon, R. A.; Phillips, A. D.; Meadows, N.; Klein, N. J.; Walker-Smith, J. A. Congenital Enterocyte Heparan Sulphate Deficiency is Associated with Massive Albumin Loss, Secretory Diarrhoea and Malnutrition. *Lancet* **1996**, *347*, 1299–1301.

(13) Valstar, A.; Almgren, M.; Brown, W.; Vasilescu, M. The Interaction of Bovine Serum Albumin with Surfactants Studied by Light Scattering. *Langmuir* **2000**, *16*, 922–927.

(14) Castelletto, V.; Krysmann, M.; Kelarakis, A.; Jauregi, P. Complex Formation of Bovine Serum Albumin with a Poly(ethylene glycol) Lipid Conjugate. *Biomacromolecules* **2007**, *8*, 2244–2249.

(15) Mukherjee, T. K.; Lahiri, P.; Datta, A. 2-(2'-Pyridyl)-Benzimidazole as a Fluorescent Probe for Monitoring Protein–Surfactant Interaction. *Chem. Phys. Lett.* **2007**, *438*, 218–223.

(16) Anand, U.; Mukherjee, S. Reversibility in Protein Folding: Effect of β -Cyclodextrin on Bovine Serum Albumin Unfolded by Sodium Dodecyl Sulphate. *Phys. Chem. Chem. Phys.* **2013**, *15*, 9375–9383.

(17) Peng, L.; Wei, R.; Li, K.; Zhou, Z.; Song, P.; Tong, A. A Ratiometric Fluorescent Probe for Hydrophobic Proteins in Aqueous Solution Based on Aggregation-Induced Emission. *Analyst* **2013**, *138*, 2068–2072.

(18) Jisha, V. S.; Arun, K. T.; Hariharan, M.; Ramaiah, D. Site-Selective Binding and Dual Mode Recognition of Serum Albumin by a Squaraine Dye. *J. Am. Chem. Soc.* **2006**, *128*, 6024–6025.

(19) Ojha, B.; Das, G. Artificial Amphiphilic Scaffolds for the Selective Sensing of Protein Based on Hydrophobicity. *Chem. Commun.* **2010**, *46*, 2079–2081.

(20) Suzuki, Y.; Yokoyama, K. Design and Synthesis of Intramolecular Charge Transfer-Based Fluorescent Reagents for the Highly-Sensitive Detection of Proteins. *J. Am. Chem. Soc.* **2005**, *127*, 17799–17802.

(21) Ghosh, S.; Guchhait, N. Chemically Induced Unfolding of Bovine Serum Albumin by Urea and Sodium Dodecyl Sulfate: A Spectral Study with the Polarity-Sensitive Charge-Transfer Fluorescent Probe (E)-3-(4-Methylaminophenyl)acrylic Acid Methyl Ester. *ChemPhysChem* **2009**, *10*, 1664–1671.

(22) Nishijima, M.; Pace, T. C. S.; Nakamura, A.; Mori, T.; Wada, T.; Bohne, C.; Inoue, Y. Supramolecular Photochirogenesis with Biomolecules. Mechanistic Studies on the Enantiodifferentiation for the Photocyclodimerization of 2-Anthracenecarboxylate Mediated by Bovine Serum Albumin. *J. Org. Chem.* **2007**, *72*, 2707–2715.

(23) Ahn, Y. H.; Lee, J. S.; Chang, Y. T. Selective Human Serum Albumin Sensor from the Screening of a Fluorescent Rosamine Library. *J. Comb. Chem.* **2008**, *10*, 376–380.

(24) Matulis, D.; Baumann, C. G.; Bloomfield, V. A.; Lovrien, R. E. 1-Anilino-8-Naphthalene Sulfonate as a Protein Conformational Tightening Agent. *Biopolymers* **1999**, *49*, 451–458.

(25) Hawe, A.; Sutter, M.; Jiskoot, W. Extrinsic Fluorescent Dyes as Tools for Protein Characterization. *Pharm. Res.* **2008**, *25*, 1487–1499.

(26) Rajasekhar, K.; Achar, C. J.; Govindaraju, T. A Red-NIR Emissive Probe for the Selective Detection of Albumin in Urine Samples and Live Cells. *Org. Biomol. Chem.* **2017**, *15*, 1584–1588.

(27) Dey, G.; Gaur, P.; Giri, R.; Ghosh, S. Optical Signaling in Biofluids: a Nondenaturing Photostable Molecular Probe for Serum Albumins. *Chem. Commun.* **2016**, *52*, 1887–1890.

(28) Zhu, T.; Du, J.; Cao, W.; Fan, J.; Peng, X. Microenvironment-Sensitive Fluorescent Dyes for Recognition of Serum Albumin in Urine and Imaging in Living Cells. *Ind. Eng. Chem. Res.* **2016**, *55*, 527–533.

(29) So, P. T. C.; Dong, C. Y.; Masters, B. R.; Berland, K. M. Two-Photon Excitation Fluorescence Microscopy. *Annu. Rev. Biomed. Eng.* **2000**, *2*, 399–429.

(30) Dumat, B.; Bordeau, G.; Faurel-Paul, E.; Mahuteau-Betzer, F.; Saettel, N.; Metge, G.; Fiorini-Debuisschert, C.; Charra, F.; Teulade-Fichou, M.-P. DNA Switches on the Two-Photon Efficiency of an Ultrabright Triphenylamine Fluorescent Probe Specific of AT Regions. *J. Am. Chem. Soc.* **2013**, *135*, 12697–12706.

(31) Schmitt, J.; Heitz, V.; Sour, A.; Bolze, F.; Kessler, P.; Flamigni, L.; Ventura, B.; Sonnet, C. S.; Toth, E. A Theranostic Agent Combining a Two-Photon-Absorbing Photosensitizer for Photodynamic Therapy and a Gadolinium (III) Complex for MRI Detection. *Chem. – Eur. J.* **2016**, *22*, 2775–2786.

(32) Hrobárik, P.; Hrobáriková, V.; Semak, V.; Kasak, P.; Rakovsky, E.; Polyzos, I.; Fakis, M.; Persephonis, P. Quadrupolar Benzobisthiazole-Cored Arylamines as Highly Efficient Two-Photon Absorbing Fluorophore. *Org. Lett.* **2014**, *16*, 6358–6361.

(33) Yao, S.; Belfield, K. D. Two-Photon Fluorescent for Bioimaging. *Eur. J. Org. Chem.* **2012**, *2012*, 3199–3217.

(34) Hrobárik, P.; Hrobáriková, V.; Sigmundová, I.; Zahradník, P.; Fakis, M.; Polyzos, I.; Persephonis, P. Benzothiazoles with Tunable Electron-Withdrawing Strength and Reverse Polarity: A Route to Triphenylamine-Based Chromophores with Enhanced Two-Photon Absorption. *J. Org. Chem.* **2011**, *76*, 8726–8736.

(35) Hrobáriková, V.; Hrobárik, P.; Gajdos, P.; Fitisil, I.; Fakis, M.; Persephonis, P.; Zahradník, P. Benzothiazole-Based Fluorophores of Donor- π -Acceptor- π -Donor Type Displaying High Two-Photon Absorption. *J. Org. Chem.* **2010**, *75*, 3053–3068.

(36) Monnereau, C.; Marotte, S.; Lanoe, P.-H.; Maury, O.; Baldeck, P.; Kreher, D.; Favier, A.; Charreyre, M.-T.; Marvel, J.; Leverrier, Y.; Andraud, C. Water-Soluble Chromophores with Star-Shaped Oligomeric Arms: Synthesis, Spectroscopic Studies and First Results in Bio-Imaging and Cell Death Induction. *New J. Chem.* **2012**, *36*, 2328–2333.

(37) Massin, J.; Charaf-Eddin, A.; Appaix, F.; Bretonniere, Y.; Jacquemin, D.; van der Sanden, B.; Monnereau, C.; Andraud, C. A Water Soluble Probe with Near Infrared Two-Photon Absorption and Polarity-Induced Fluorescence for Cerebral Vascular Imaging. *Chem. Sci.* **2013**, *4*, 2833–2843.

(38) Mettra, B.; Appaix, F.; Olesiak-Banska, J.; Le Bahers, T.; Leung, A.; Matczyszyn, K.; Samoc, M.; van der Sanden, B.; Monnereau, C.; Andraud, C. A Fluorescent Polymer Probe with High Selectivity toward Vascular Endothelial Cells for and beyond Noninvasive Two-Photon Intravital Imaging of Brain Vasculature. *ACS Appl. Mater. Interfaces* **2016**, *8*, 17047–17059.

(39) Kunz, H.; Mullen, K. Natural Product and Material Chemistries—Separated Forever? *J. Am. Chem. Soc.* **2013**, *135*, 8764–8769.

(40) Hilderbrand, S. A.; Weissleder, R. Near-Infrared Fluorescence: Application to In Vivo Molecular Imaging. *Curr. Opin. Chem. Biol.* **2010**, *14*, 71–79.

(41) Deiana, M.; Mettra, B.; Matczyszyn, K.; Piela, K.; Pitrat, D.; Olesiak-Banska, J.; Monnereau, C.; Andraud, C.; Samoc, M. Interactions of a Biocompatible Water-Soluble Anthracenyl Polymer Derivative with Double-Stranded DNA. *Phys. Chem. Chem. Phys.* **2015**, *17*, 30318–30327.

(42) Deiana, M.; Mettra, B.; Matczyszyn, K.; Pitrat, D.; Olesiak-Banska, J.; Monnereau, C.; Andraud, C.; Samoc, M. Unravelling the Binding Mechanism of a Poly(cationic) Anthracenyl Fluorescent Probe with High Affinity toward Double-Stranded DNA. *Biomacromolecules* **2016**, *17*, 3609–3618.

(43) Ibrahim, N.; Ibrahim, H.; Kim, S.; Nallet, J.-P.; Nepveu, F. Interactions between Antimalarial Indolone-N-oxide Derivatives and Human Serum Albumin. *Biomacromolecules* **2010**, *11*, 3341–3351.

(44) Martínez-Tomé, M. J.; Esquembre, R.; Mallavia, R.; Mateo, C. R. Formation of Complexes between the Conjugated Polyelectrolyte Poly{[9,9-bis(6'-N,N,N-trimethylammonium)hexyl]fluorene-phenylene} Bromide (HTMA-PFP) and Human Serum Albumin. *Biomacromolecules* **2010**, *11*, 1494–1501.

(45) Lakowicz, J. R. *Principles of Fluorescence Spectroscopy*, 3rd ed.; Springer: New York, 2006.

- (46) Deiana, M.; Matczyszyn, K.; Massin, L.; Olesiak-Banska, J.; Andraud, C.; Samoc, M. Interactions of Isophorone Derivatives with DNA: Spectroscopic Studies. *PLoS One* **2015**, *10*, No. e0129817.
- (47) Kamal, A. J.; Behere, D. V. Spectroscopic Studies on Human Serum Albumin and Methemalbumin: Optical, Steady-State, and Picosecond Time-Resolved Fluorescence Studies, and Kinetics of Substrate Oxidation by Methemalbumin. *J. Biol. Inorg. Chem.* **2002**, *7*, 273–283.
- (48) El-Kemary, M.; Gil, M.; Douhal, A. Relaxation Dynamics of Piroxicam Structures within Human Serum Albumin Protein. *J. Med. Chem.* **2007**, *50*, 2896–2902.
- (49) Deiana, M.; Pokladek, Z.; Ziemianek, M.; Tarnowicz, N.; Mlynarz, P.; Samoc, M.; Matczyszyn, K. Probing the Binding Mechanism of Photoresponsive Azobenzene Polyamine Derivatives with Human Serum Albumin. *RSC Adv.* **2017**, *7*, 5912–5919.
- (50) Hu, Y.-J.; Liu, Y.; Xiao, X.-H. Investigation of the Interaction between Berberine and Human Serum Albumin. *Biomacromolecules* **2009**, *10*, 517–521.
- (51) Deiana, M.; Pokladek, Z.; Olesiak-Banska, J.; Mlynarz, P.; Samoc, M.; Matczyszyn, K. Photochromic Switching of the DNA Helicity Induced by Azobenzene Derivatives. *Sci. Rep.* **2016**, *6*, No. 28605.
- (52) Deiana, M.; Pokladek, Z.; Matczyszyn, K.; Mlynarz, P.; Buckle, M.; Samoc, M. Effective Control of the Intrinsic DNA Morphology by Photosensitive Polyamines. *J. Mater. Chem. B* **2017**, *5*, 1028–1038.
- (53) Chakrabarty, A.; Mallick, A.; Halder, B.; Das, P.; Chattopadhyay, N. Binding Interaction of a Biological Photosensitizer with Serum Albumins: A Biophysical Study. *Biomacromolecules* **2007**, *8*, 920–927.
- (54) Chi, Z.; Liu, R. Phenotypic Characterization of the Binding of Tetracycline to Human Serum Albumin. *Biomacromolecules* **2011**, *12*, 203–209.
- (55) Beauchemin, R.; N'soukpoe-Kossi, C. N.; Thomas, T. J.; Thomas, T.; Carpentier, R.; Tajmir-Riahi, H. A. Polyamine Analogues Bind Human Serum Albumin. *Biomacromolecules* **2007**, *8*, 3177–3183.
- (56) Sharma, A. S.; Anandakumar, S.; Ilanchelian, M. *In vitro* Investigation of Domain Specific Interactions of Phenothiazine Dye with Serum Proteins by Spectroscopic and Molecular Docking Approaches. *RSC Adv.* **2014**, *4*, 36267–36281.
- (57) Bourassa, P.; Kanakis, C. D.; Tarantilis, P.; Pollissiou, M. G.; Tajmir-Riahi, H. A. Resveratrol, Genistein, and Curcumin Bind Bovine Serum Albumin. *J. Phys. Chem. B* **2010**, *114*, 3348–3354.
- (58) Cheng, Z. Comparative Studies on the Interactions of Honokiol and Magnolol With Human Serum Albumin. *J. Pharm. Biomed. Anal.* **2012**, *66*, 240–251.
- (59) Dubeau, S.; Bourassa, P.; Thomas, T. J.; Tajmir-Riahi, H. A. Biogenic and Synthetic Polyamines Bind Bovine Serum Albumin. *Biomacromolecules* **2010**, *11*, 1507–1515.
- (60) Lin, S.-Y.; Wei, Y.-S.; Li, M.-J.; Wang, S.-L. Effect of Ethanol or/and Captopril on the Secondary Structure of Human Serum Albumin Before and After Protein Binding. *Eur. J. Pharm. Biopharm.* **2004**, *57*, 457–464.
- (61) Juárez, J.; Taboada, P.; Mosquera, V. Existence of Different Structural Intermediates on the Fibrillation Pathway of Human Serum Albumin. *Biophys. J.* **2009**, *96*, 2353–2370.
- (62) Förster, T. Zwischenmolekulare Energiewanderung und Fluoreszenz. *Ann. Phys.* **1948**, *437*, 55–75.
- (63) Chung, C. Y.-S.; Yam, V. W.-W. Induced Self-Assembly and Förster Resonance Energy Transfer Studies of Alkynylplatinum(II) Terpyridine Complex Through Interaction With Water-Soluble Poly(phenylene ethynylene sulfonate) and the Proof-of-Principle Demonstration of this Two-Component Ensemble for Selective Label-Free Detection of Human Serum Albumin. *J. Am. Chem. Soc.* **2011**, *133*, 18775–18784.
- (64) Rehman, M. T.; Shamsi, H.; Khan, U. Insight into the Binding Mechanism of Imipenem to Human Serum Albumin by Spectroscopic and Computational Approaches. *Mol. Pharmaceutics* **2014**, *11*, 1785–1797.
- (65) Feroz, S. R.; Mohamad, S. B.; Bakri, Z. S. D.; Malek, S. N. A.; Tayyab, S. Probing the Interaction of a Therapeutic Flavonoid, Pinostrobin with Human Serum Albumin: Multiple Spectroscopic and Molecular Modeling Investigations. *PLoS One* **2013**, *8*, No. e76067.
- (66) Ganguly, A.; Ghosh, S.; Guchhait, N. Spectroscopic and Viscometric Elucidation of the Interaction between a Potential Chloride Channel Blocker and Calf-Thymus DNA: the Effect of Medium Ionic Strength on the Binding Mode. *Phys. Chem. Chem. Phys.* **2015**, *17*, 483–492.
- (67) Wang, Y.-R.; Feng, L.; Xu, L.; Li, Y.; Wang, D.-D.; Hou, J.; Zhou, K.; Jin, Q.; Ge, G.-B.; Cui, J.-N.; Yang, L. A Rapid-Response Fluorescent Probe for the Sensitive and Selective Detection of Human Albumin in Plasma and Cell Culture Supernatants. *Chem. Commun.* **2016**, *52*, 6064–6067.
- (68) Thomsen, V.; Schatzlein, D.; Mercurio, D. Limits of Detection in Spectroscopy. *Spectroscopy* **2003**, *18*, 112–114.
- (69) Greenfield, N. J. Using Circular Dichroism Spectra to Estimate Protein Secondary Structure. *Nat. Protoc.* **2006**, *1*, 2876–2890.